ISSN 1063-7788, Physics of Atomic Nuclei, 2021, Vol. 84, No. 5, pp. 635–642. © Pleiades Publishing, Ltd., 2021.
Russian Text © The Author(s), 2021, published in Yadernaya Fizika, 2021, Vol. 84, No. 5, pp. 402–409.

NUCLEI
Experiment

Dynamics of the Neutron Transfer Process in the Reaction ^{181}Ta(^{18}O, ^{19}O) at an Energy of 10 MeV per Nucleon

A. K. Azhibekov[1),2),3)*], Yu. E. Penionzhkevich[1),4)], S. M. Lukyanov[1)], T. Issatayev[1),3),5)], V. A. Maslov[1)], K. Mendibayev[1),3)], M. A. Naumenko[1)], N. K. Skobelev[1)], K. A. Kuterbekov[5)], and A. M. Mukhambetzhan[2)]

Received November 11, 2020; revised December 2, 2020; accepted December 3, 2020

Abstract—The results of an experiment carried out on the MAVR high-resolution magnetic spectrometer and devoted to studying neutron transfer in the ^{18}O+^{181}Ta reaction at the projectile energy of 10 MeV per nucleon are presented. A theoretical analysis of the experimental cross sections is performed for the neutron transfer mechanism by means of a time-dependent approach based on solving the time-dependent Schrödinger equation. The dynamics of the neutron transfer process is described, and the probabilities for the population of unoccupied neutron levels in the ^{19}O nucleus are determined.

DOI: 10.1134/S1063778821040074

1. INTRODUCTION

This article reports on the results of experimental investigations and theoretical calculations of the neutron transfer reaction leading to the production of nuclei of the light neutron-rich oxygen isotope ^{19}O. The theoretical calculations are carried out within a time-dependent approach based on solving the time-dependent Schrödinger equation. Analysis of nucleon-transfer reactions is an important line of research in heavy-ion physics, since it allows one to estimate the potential of such reactions for synthesizing new exotic nuclei. Theoretical studies of the mechanisms of neutron transfer reactions are of great importance for planning and performing experiments aimed at the production of neutron-rich nuclei in the vicinity of the nucleon drip line. In addition, such studies may be useful for further advancement to the region of nuclear instability, where nuclei exist in the form of resonances in the continuum (for example, the oxygen isotopes ^{25,26}O) and have characteristic nuclear lifetimes.

[1)]Joint Institute for Nuclear Research, Dubna, Russia.
[2)]Korkyt Ata Kyzylorda University, Kyzylorda, Republic of Kazakhstan.
[3)]Institute of Nuclear Physics, Ministry of Energy of Republic of Kazakhstan, Almaty, Republic of Kazakhstan.
[4)]National Research Nuclear University MEPhI, Moscow, Russia.
[5)]L.N. Gumilyov Eurasian National University, Nur-Sultan, Republic of Kazakhstan.
[*]E-mail: azhibekoaidos@mail.ru

2. IMPLEMENTATION OF THE EXPERIMENT

In [1, 2], our group published the results of an experiment performed on the MAVR high-resolution magnetic spectrometer, which played the role of a magnetic analyzer, and devoted to measuring the differential cross sections for the production of the neutron-rich oxygen isotopes $^{18-22}$O in the ^{18}O+^{181}Ta reaction at the energy of 10 MeV per nucleon. This experiment was conducted at the U-400 cyclotron of the Flerov Laboratory of Nuclear Reactions (FLNR) at the Joint Institute for Nuclear Research (JINR, Dubna). We have studied neutron transfer channels with ^{18}O beams and ^{181}Ta target nuclei. In order to form a beam profile, we used the magnetic optics of the beam extraction line of the U-400 cyclotron, supplemented with a set of diaphragms. The beam profile was monitored by means of dedicated profilometers. As a result, we were able to obtain a beam of cross-sectional area 5×5 mm and intensity 100 nA at the target. A ^{181}Ta target with thickness 4 μm was used in the experiment. The MAVR magnetic analyzer made it possible to separate reaction products and beam nuclei with a rather high efficiency (the solid angle was 1.5 msr). The range of energies of reaction products that could be detected by the spectrometer was $E_{\max}/E_{\min} = 5.2$ with the energy resolution of $\Delta E/E = 5 \times 10^{-4}$. A system for analysis and detection of particles made it possible to measure the energy spectra of reaction products in the range between 30 and 110 MeV. The MAVR magnetic analyzer for registering reaction products provides

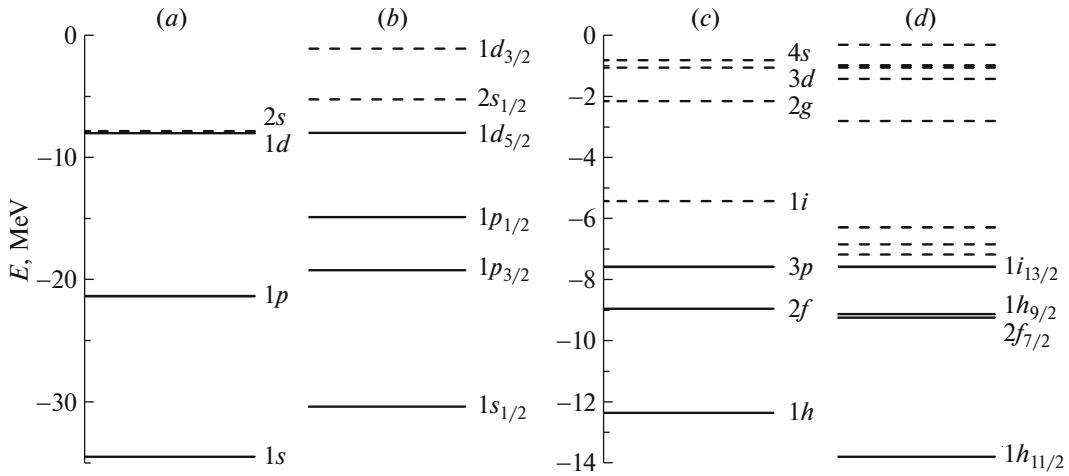

Fig. 1. (*a*, *b*) Single-particle neutron energy levels in the ^{18}O nucleus and (*c*, *d*) upper levels in the ^{181}Ta nucleus within the shell model of spherical nuclei (*a*, *c*) without and (*b*, *d*) with spin–orbit interaction.

the possibility of working at low angles with beams of high intensity (up to 5×10^{12} s^{-1}). The trajectories of beam charged states and nuclear-reaction products were determined by calculations. The positions of all reaction products in the spectrometer focal plane were determined by means of position-sensitive detectors.

3. THEORETICAL ANALYSIS OF EXPERIMENTAL RESULTS

In [1, 2], we performed a theoretical analysis of our experimental results in the Distorted-Wave Born Approximation (DWBA). An analysis of nucleon-transfer reactions within a precise quantum-mechanical description of transferred particles seems to be more correct. This is possible by the numerical solution of the time-dependent Schrödinger equation for nucleon wave functions in the mean field of nuclei moving along classical trajectories [3–8]. The use of this time-dependent method provides visualization of the dynamics of occurring processes and fast calculations on a mesh with a step of 0.1 to 0.3 fm, which is smaller than the spacing between the probability density oscillations for single-particle states. This allows one to calculate quite precisely the spatial structure of neutron wave functions. In the following, we examine one-neutron transfer reactions the interaction of ^{18}O and ^{181}Ta, relying on this method.

The structure of the ^{18}O and ^{181}Ta nuclei was determined within the shell model for spherical nuclei with and without spin–orbit interaction [9] (see Fig. 1). The parameters of the Woods–Saxon potential (see Table 1) were chosen by fitting the energies of the upper occupied neutron levels in the ^{18}O and ^{181}Ta nuclei to the sign-reversed neutron separation energies. The experimental values of the neutron separation energies for the ^{18}O and ^{181}Ta nuclei are, respectively, 8.045 and 7.576 MeV [10]. Figure 1 shows that the structure of the upper occupied neutron levels of the ^{181}Ta nucleus in the shell model with and without spin–orbit interaction is similar. In order to obtain deeper qualitative insight into the neutron transfer process and to reduce substantially the time for numerical solution of the time-dependent Schrödinger equation, we disregarded the neutron spin, and this did not lead to significant changes in the results, as in [3, 7, 8].

The radial parts $R_{n\,l}(r)$ of the wave functions for the upper neutron levels of the ^{18}O and ^{181}Ta nuclei in the shell model without spin–orbit interaction are shown in Fig. 2.

Figure 3 provides examples of the calculation of the wave-function probability density $|\psi_{n\,l\,m}(\mathbf{r})|^2$ for a neutron in the $3p$ shell of the ^{181}Ta nucleus with the angular momentum projections $m_l = 0, \pm 1$ onto the z axis and the m_l-averaged wave-function probability density

$$|\psi_{3p}(\mathbf{r})|^2 = \frac{1}{3}\Big[\,|\psi_{3p\,m_l=0}(\mathbf{r})|^2 + |\psi_{3p\,m_l=+1}(\mathbf{r})|^2 + |\psi_{3p\,m_l=-1}(\mathbf{r})|^2\Big]. \quad (1)$$

The wave functions $\psi_{3p\,m_l=0,\pm1}(\mathbf{r})$ were used as the initial states of the neutron for solving the time-dependent Schrödinger equation describing the evolution of the wave function $\Psi(\mathbf{r}, t)$ for the outer neutron in the field of colliding nuclei; that is,

$$i\hbar\frac{\partial\Psi}{\partial t} = -\frac{\hbar^2}{2m}\Delta\Psi + \left(V_1\left(|\mathbf{r}-\mathbf{r}_1(t)|\right) + V_2\left(|\mathbf{r}-\mathbf{r}_2(t)|\right)\right)\Psi, \quad (2)$$

Table 1. Parameters of the Woods–Saxon potential for ^{18}O and ^{181}Ta nuclei in the shell model of spherical nuclei with and without spin–orbit interaction [9] (κ is the spin–orbit coupling constant)

Nucleus	$V_0^{(\mathrm{WS})}$, MeV	$r_0^{(\mathrm{WS})}$, fm	$a^{(\mathrm{WS})}$, fm	$V_0^{(\mathrm{SO})}$, MeV	$r_0^{(\mathrm{SO})}$, fm	$a^{(\mathrm{SO})}$, fm	κ
^{18}O	−47.350	1.347	0.7	−44.86	1.31	0.7	35
^{18}O	−52.069	1.347	0.7	–	–	–	–
^{181}Ta	−42.050	1.347	0.7	−41.35	1.31	0.7	35
^{181}Ta	−42.747	1.347	0.7	–	–	–	–

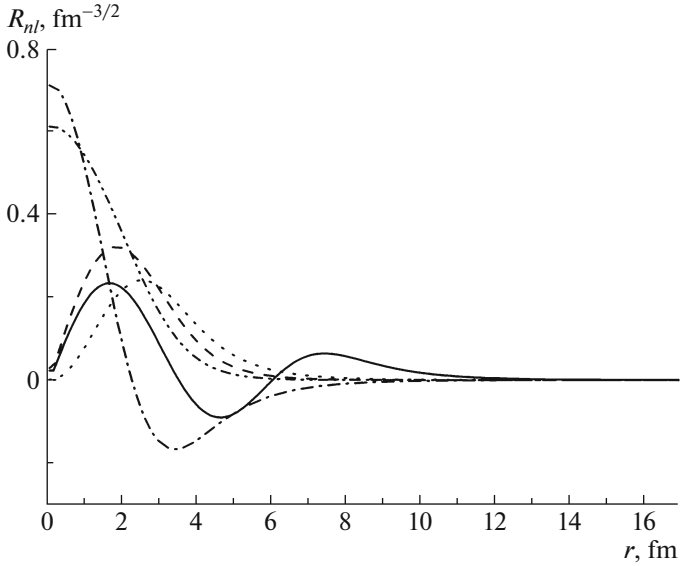

Fig. 2. Radial parts $R_{nl}(r)$ of the wave functions for the upper neutron levels in the shell model without spin–orbit interaction for the $1s$ (dash-dot-dotted curve), $1p$ (dashed curve), $1d$ (dotted curve), and $2s$ (dash-dotted curve) states in the ^{18}O nucleus and the $1p$ (solid curve) state in the ^{181}Ta nucleus.

where $\mathbf{r}_1(t)$ and $\mathbf{r}_2(t)$ are the radius vectors of the centers of colliding nuclei with masses m_1 and m_2 moving along classical trajectories, m is the nucleon mass, and $V_i(|\mathbf{r}-\mathbf{r}_i(t)|)$ stands for the mean-field potentials of neutron–nucleus interaction. The time dependence of the neutron potential energy is determined by the motion of nuclei in their center-of-mass frame. In order to solve Eq. (2), we used a uniform spatial mesh in the three-dimensional system of Cartesian coordinates (x, y, z) with the dimensions of the mesh $285 \times 200 \times 435$ points ($85 \times 60 \times 130.5$ fm^3). For constructing a numerical solution, a spatial mesh is usually taken in the form of a rectangular parallelepiped whose dimensions are chosen in such a way as to meet the requirements of a specific problem. Here, we set the spatial mesh step to 0.3 fm, which is much smaller than the nuclear size—that is, a characteristic scale over which the total wave function for stationary states and its radial part change strongly. The calculations were performed at the HybriLIT heterogeneous computing cluster of JINR [11].

Solving the equations

$$m_1\ddot{\mathbf{r}}_1 = -\nabla_{\mathbf{r}_1}U(|\mathbf{r}_1-\mathbf{r}_2|),$$
$$m_2\ddot{\mathbf{r}}_2 = -\nabla_{\mathbf{r}_2}U(|\mathbf{r}_1-\mathbf{r}_2|), \qquad (3)$$

we calculated the trajectories of the ^{18}O and ^{181}Ta nuclei in their center-of-mass frame (see Fig. 4a). Figure 4 shows that, for the chosen trajectories of a grazing collision between the nuclei, the minimal distance between their centers as they approached each other, $R_{\min}$, was larger than the sum of their root-mean-square charge radii, which is 8.12 fm (2.77 fm for the ^{18}O nucleus and 5.35 fm for the ^{181}Ta nucleus [10]). For the central part of the nucleus–nucleus interaction potential, $U(|\mathbf{r}_2-\mathbf{r}_1|)$, in the Woods–Saxon form, we used the same parameter values as in the DWBA calculations performed earlier and reported in [1, 2]: $V_{N0} = -63.487$ MeV, $R_N = 9.753$ fm, and $a_N = 0.659$ fm, which yielded

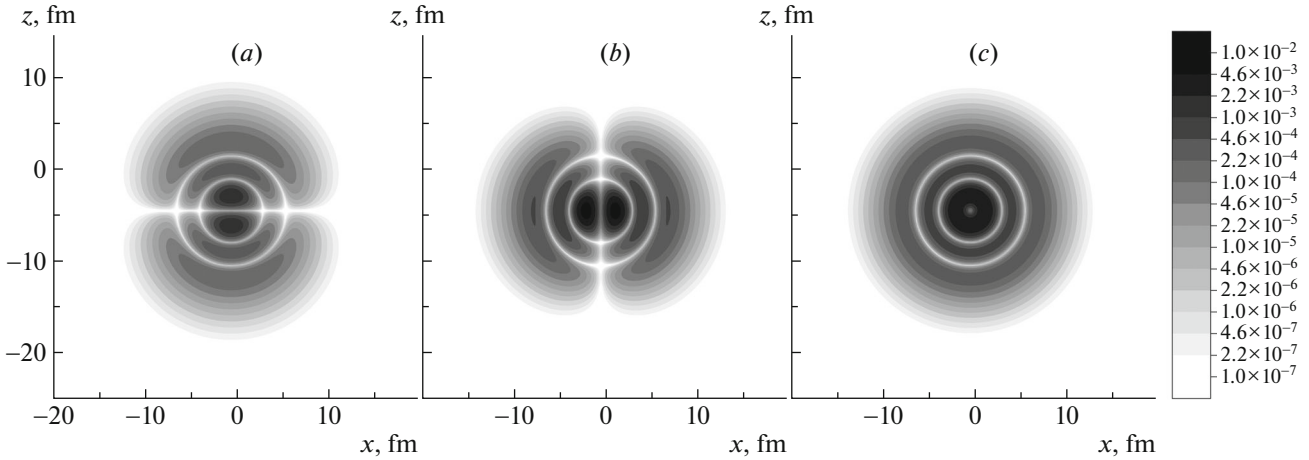

Fig. 3. (a, b) Wave-function probability densities $|\Psi_{n\,l\,m_l}(\mathbf{r})|^2$ for a neutron in the $3p$ shell of the ^{181}Ta nucleus for the angular momentum projections (a) $m_l = 0$ and (b) $m_l = \pm 1$; (c) neutron probability density averaged over the angular momentum projections.

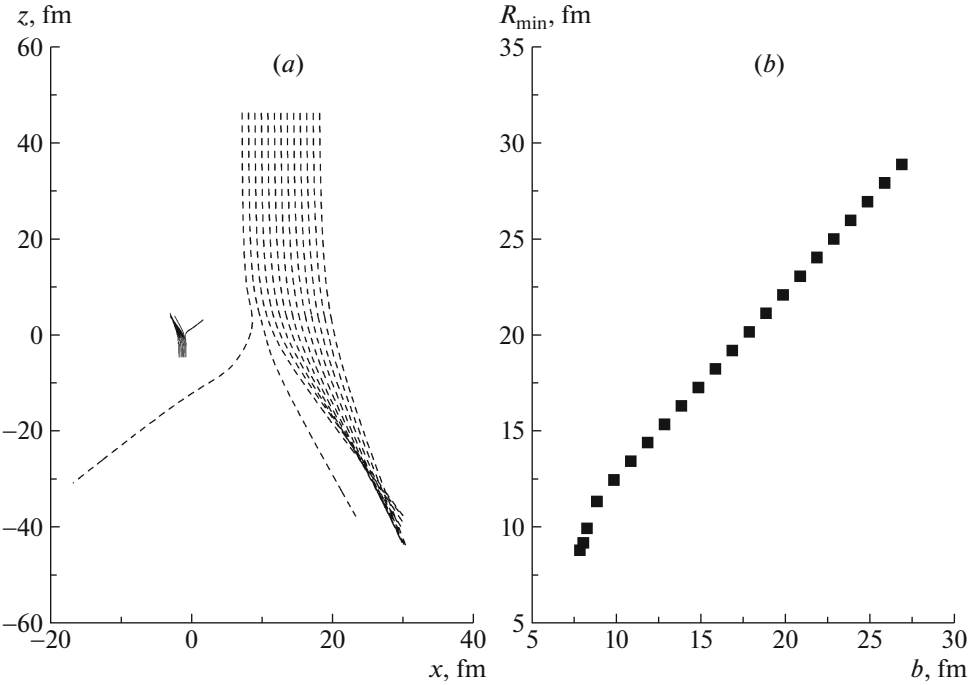

Fig. 4. Collisions of ^{18}O and ^{181}Ta nuclei at the energy of 10 MeV per nucleon (163.72 MeV in the center-of-mass frame): (a) trajectories of motion of the (dashed curves) ^{18}O and (solid curves) ^{181}Ta nuclei for the impact parameter values in the range of $b = 7.85$–20.85 fm and (b) $R_{\min}$ as a function of the impact parameter b.

the Coulomb barrier height $V_B = 68.94$ MeV. The dependence of $R_{\min}$ on the impact-parameter b for the ^{18}O and ^{181}Ta nuclei from the calculation of the trajectories in the center-of-mass frame is shown in Fig. 4b. Using the projections of the velocity vector of the ^{18}O projectile nucleus found by numerical solution of Eq. (3), we determined the scattering angles in the center-of-mass frame of colliding nuclei, $\theta_{\text{c.m.}}$, and in the laboratory frame, θ_{lab}.

The experimental differential cross sections for the neutron transfer channel leading to the formation of oxygen isotopes were obtained for an angle of $\theta_{\text{lab}} = 12^\circ$ ($\theta_{\text{c.m.}} = 13.9^\circ$). The corresponding trajectories are characterized by the impact parameter value of $b = 8.6$ fm. An example of the evolution of the probability density for the outer neutron of the ^{181}Ta nucleus in the course of a grazing collision of the ^{18}O and ^{181}Ta nuclei at $b = 8.6$ fm is given in Fig. 5. It can

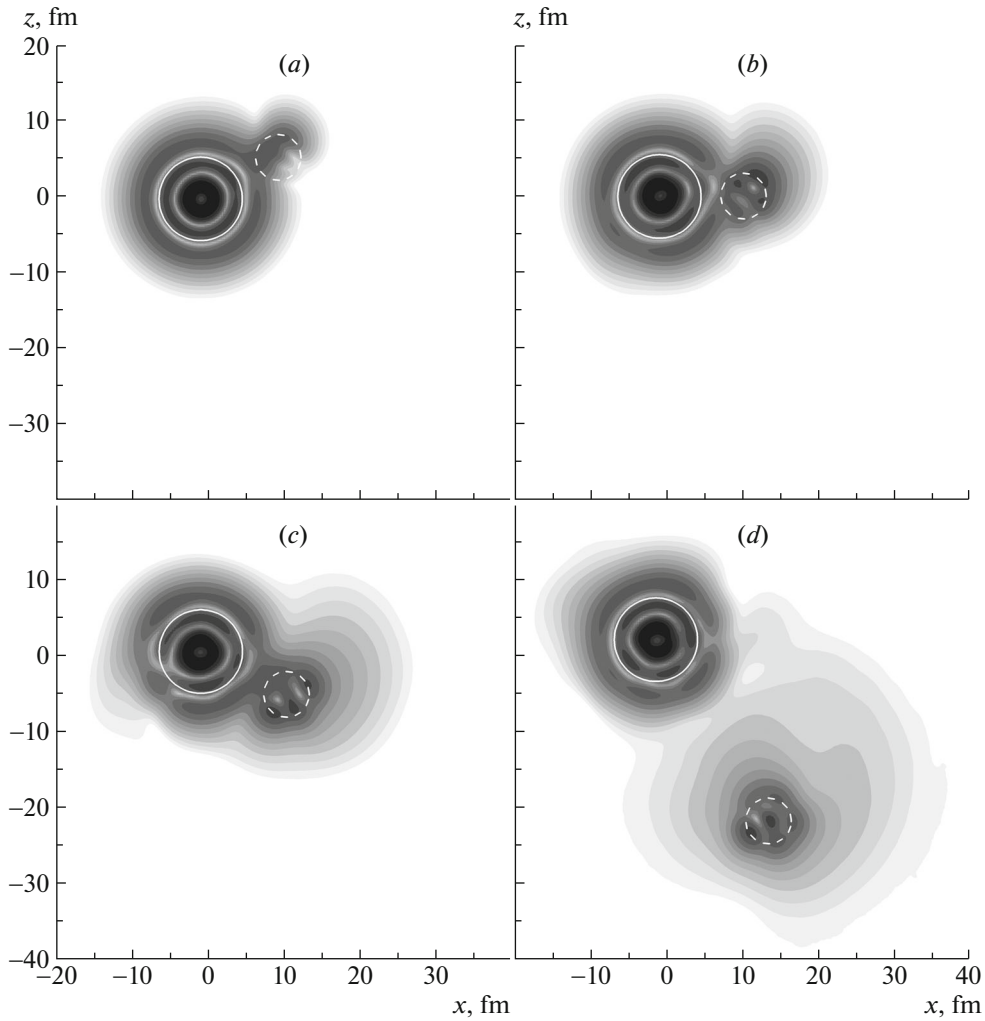

Fig. 5. Evolution of the probability density for the outer neutron of the ^{181}Ta nucleus in the course of a grazing collision of ^{18}O (dashed-line circle) with ^{181}Ta (solid-line circle). The radii of the circles are equal to the root-mean-square charge radii of the nuclei, the impact parameter is $b = 8.6$ fm, and $E_{\text{c.m.}} = 163.72$ MeV. The order of the panels (a, b, c, and d) corresponds to the course of time.

be seen that the flux of the probability density from the ^{181}Ta nucleus to the ^{18}O nucleus is somewhat shifted off the center-to-center axis of the nuclei (Fig. 5a). Because of a high relative velocity of motion of the nuclei, the neutron does not have time to go over to the ^{18}O nucleus and to populate the unoccupied levels of the bound state. In the course of time, a major part of the transferred probability density leaves the ^{18}O nucleus, going over to states of continuous energy spectrum (see Fig. 5d).

In order to estimate quantitatively the probability that a neutron populates the unoccupied $1p$, $1d$, and $2s$ states in the ^{18}O projectile nucleus, we expand the neutron wave function into the wave functions for neutron states in a nucleus moving with a velocity ν_1; that is,

$$\Psi(\mathbf{r},t) = \sum_{n l m_l} a_{n l m_l} \psi_{n l m_l}(\mathbf{r} - \mathbf{r}_1) \times \exp\left(i\frac{m\nu_1 \mathbf{r}}{\hbar}\right). \quad (4)$$

The expansion coefficients $a_{n l m_l}$ with complex values are given by

$$a_{n l m_l} = \int\limits_{S_1} \left[\psi_{n l m_l}(\mathbf{r} - \mathbf{r}_1) \times \exp\left(i\frac{m\nu_1 \mathbf{r}}{\hbar}\right)\right]^* \Psi(\mathbf{r},t) dV, \quad (5)$$

where S_1 is a sphere centered at $\mathbf{r}_1(t)$ with radius $r_1 =$ 10 fm. The squared modulus of the expansion coefficients $a_{n l m_l}$ determines the probability with which

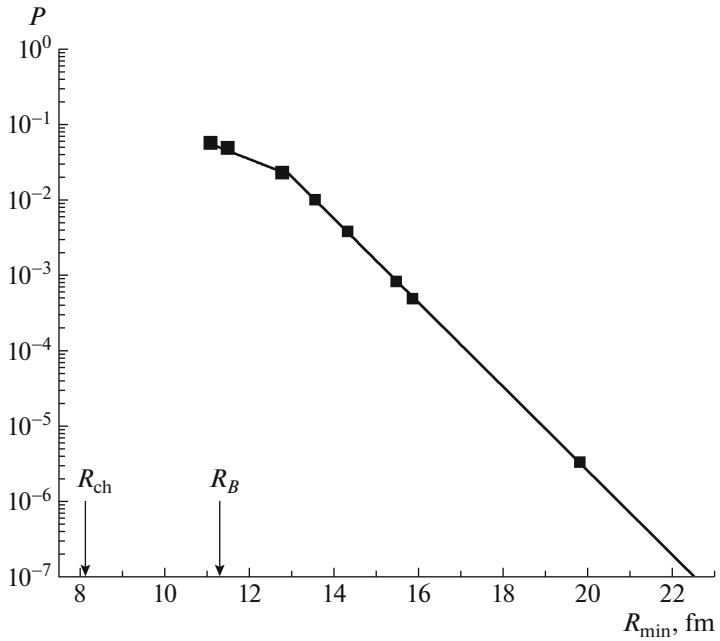

Fig. 6. Neutron transfer probability P as a function of $R_{\min}$ for the reaction ^{181}Ta(^{18}O, ^{19}O)^{180}Ta. Here, R_{ch} is the sum of the root-mean-square charge radii of the nuclei, R_B is the Coulomb barrier radius.

the transferred particle occupies the state characterized by the quantum numbers n, l, and m_l. Thus, the weight $w_{n\,l}$ of the state is calculated by the formula

$$w_{n\,l} = \sum_{m_l=-1}^{1} |a_{n\,l\,m_l}|^2. \qquad (6)$$

The probability of neutron transfer to the ^{18}O projectile nucleus is given by

$$p_{\rm tr} = \int\limits_{S_1} |\Psi|^2\, dV. \qquad (7)$$

For ^{18}O+^{181}Ta collisions at the energy of $E_{\rm c.m.} = 163.72$ MeV and the value of the impact parameter $b = 8.6$ fm (see Fig. 5d), the probabilities for the population of the states of the ^{18}O nucleus are the following: $w_{1p}/p_{\rm tr} \approx 0.02$ for the $1p$ state, $w_{1d}/p_{\rm tr} \approx 0.15$ for the $1d$ state, and $w_{2s}/p_{\rm tr} \approx 0.26$ for the $2s$ state. Some part (about 0.57) of the transferred neutron cloud corresponds to quasistationary states of ^{18}O. The probability for the population of deep states of ^{18}O is rather low.

For $b = 8.6$ fm and $R_{\min} = 10.94$ fm, the neutron transfer probability is $p_{\rm tr} = 0.056$. The dependence of this probability on $R_{\min}$ is shown in Fig. 6. At larger values of b and $R_{\min}$, the logarithm of the transfer probability decreases linearly by several orders of magnitude. The probability calculated for neutron transfer in the course of a collision of the nuclei at the large values of $b = 22.5$ fm and $R_{\min} = 24.64$ fm, which correspond to $\theta_{\rm c.m.} = 13.19°$, is insignificant.

The experimental value of the differential cross section for the neutron transfer channel ^{181}Ta(^{18}O, ^{19}O) at $\theta_{\rm c.m.} = 13.9°$ and $E_{\rm c.m.} = 163.72$ MeV is 0.309 ± 0.071 mb (see Fig. 7) with the relative measurement error about 23.1% [1, 2]. In order to calculate the theoretical value of the differential cross section for neutron transfer, we make use of the following formula for the differential cross section for elastic scattering in classical mechanics:

$$\frac{d\sigma}{d\Omega}(\theta_{\rm c.m.}) = \frac{b(\theta_{\rm c.m.})}{\sin\theta_{\rm c.m.}} \left|\frac{db(\theta_{\rm c.m.})}{d\theta_{\rm c.m.}}\right|. \qquad (8)$$

Multiplying the cross section in (8) by the neutron transfer probability $p_{\rm tr}$, we obtain the theoretical value of the differential cross section for neutron transfer; that is,

$$\frac{d\sigma_{\rm tr}}{d\Omega}(\theta_{\rm c.m.}) = \frac{d\sigma}{d\Omega}(\theta_{\rm c.m.})\, p_{\rm tr}(b(\theta_{\rm c.m.}))\,. \qquad (9)$$

For an angle of $\theta_{\rm c.m.} = 13.9°$, the theoretical neutron transfer cross section calculated according to Eqs. (8) and (9) is 0.201 mb.

In Fig. 7, the experimental differential cross sections for neutron transfer are compared with their theoretical counterparts obtained by applying the DWBA method [1] and by numerical solution of the time-dependent Schrödinger equation. This figure shows that both theoretical cross sections are close to the

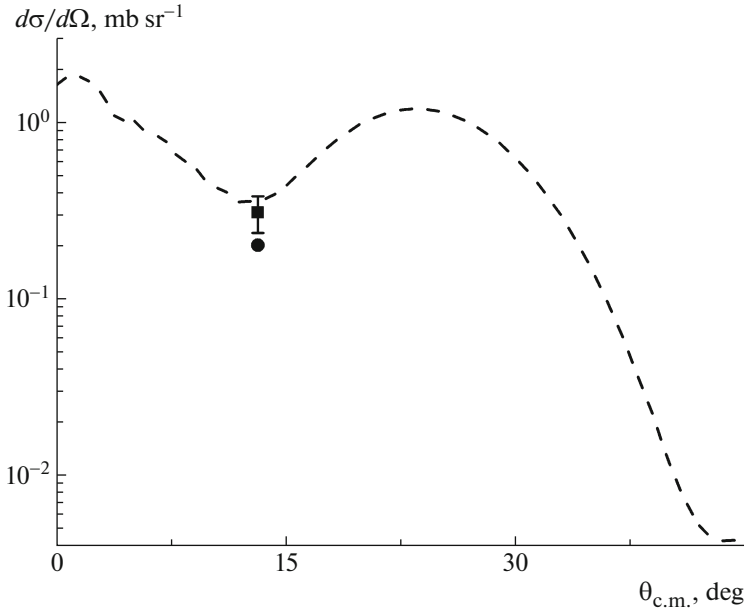

Fig. 7. Differential cross sections for the neutron transfer channel ^{181}Ta(^{18}O, ^{19}O)^{180}Ta at the energy of 10 MeV per nucleon: (filled square) experimental data from [1, 2], (dashed curve) results of the DWBA calculation from [1] for neutron transfer, and (filled circle) results obtained by means of the time-dependent approach.

experimental one. Thus, one can see that, by applying the above two complementary approaches—the DWBA method (for calculating the angular distribution of the reaction cross sections) and the time-dependent approach (making it possible to visualize reaction dynamics and to determine the mechanism of population of neutron states (see Fig. 7))—we were able to obtain both a quantitative and a qualitative description of the neutron transfer reaction.

4. CONCLUSIONS

The experimental data obtained earlier at the U-400 cyclotron of the Flerov Laboratory of Nuclear Reactions at JINR by means of the MAVR high-resolution magnetic analyzer have been described within the approach based on numerical solution of the time-dependent Schrödinger equation. The theoretical differential cross section obtained in this way for the neutron transfer channel ^{181}Ta(^{18}O, ^{19}O)^{180}Ta at the energy of 10 MeV per nucleon is close to the respective experimental cross section.

The proposed approach has made it possible to describe the dynamics of the neutron transfer process and to determine the probabilities for the population of unoccupied levels in the ^{19}O nucleus. At an energy of 10 MeV per nucleon, most part (about 57%) of the transferred neutron cloud corresponds to quasi-stationary states.

Our theoretical analysis of the neutron transfer mechanism within the time-dependent approach used has revealed that, in the energy region of $E >$ 10 MeV per nucleon, the flux of the neutron probability density from the ^{181}Ta nucleus to the ^{18}O nucleus is shifted off the center-to-center axis of colliding nuclei. From the point of view of the production of neutron-rich nuclei, reactions at energies in the range of $E < 10$ MeV per nucleon can therefore be thought to be more promising, since intense transfer and an efficient population of single-particle levels by neutrons are expected in them owing to the motion of colliding nuclei at lower relative velocities, in which case the flux of the probability density is not shifted off the center-to-center axis.

ACKNOWLEDGMENTS

The authors thank the team of the HybriLIT heterogeneous computing cluster of JINR for help in performing cumbersome computer calculations.

REFERENCES

1. A. K. Azhibekov, V. A. Zernyshkin, V. A. Maslov, Yu. E. Penionzhkevich, K. Mendibaev, T. Isataev, M. A. Naumenko, N. K. Skobelev, S. Stukalov, and D. Aznabaev, Phys. At. Nucl. **83**, 93 (2020).
2. Yu. E. Penionzhkevich, S. M. Lukyanov, A. K. Azhibekov, M. A. Naumenko, T. Issatayev, I. V. Kolesov, V. A. Maslov, K. Mendibayev,

V. A. Zernyshkin, K. A. Kuterbekov, and A. M. Mukhambetzhan, J. Phys.: Conf. Ser. **1555**, 012031 (2020).
3. V. I. Zagrebaev, V. V. Samarin, and W. Greiner, Phys. Rev. C **75**, 035809 (2007).
4. V. I. Zagrebaev and V. V. Samarin, Phys. At. Nucl. **70**, 1003 (2007).
5. V. V. Samarin, Bull. Russ. Acad. Sci.: Phys. **84**, 990 (2020).
6. V. V. Samarin, Phys. At. Nucl. **81**, 486 (2018).
7. A. K. Azhibekov, V. V. Samarin, and K. A. Kuterbekov, Eurasian J. Phys. Funct. Mater. **4**, 19 (2020).
8. A. K. Azhibekov, V. V. Samarin, and K. A. Kuterbekov, Chin. J. Phys. **65**, 292 (2020).
9. A. K. Azhibekov, V. V. Samarin, K. A. Kuterbekov, M. A. Naumenko, Eurasian J. Phys. Funct. Mater. **3**, 307 (2019).
10. NRV Web Knowledge Base on Low-Energy Nuclear Physics. http://nrv.jinr.ru/.
11. HybriLIT Heterogeneous Computing Cluster of JINR Information Technology Laboratory. http://hybrilit.jinr.ru/.